Supplementary Information

A Flexible, Integrated Film Battery Configuration for Ultrafast Sodium Ion Storage

Wenyu Zhao,[a] Helin Wang,[a] Shaowen Li,[a] Xiaoyu Tang,[a] Min Zhang,[a] Ali Mustehsin,[a]

Miao Bai,[a] Siyuan Liu,[a] Changchun Sun [a] and Yue Ma[a]*

[a] State Key Laboratory of Solidification Processing, Centre for Nano Energy Materials,

School of Materials Science and Engineering, Northwestern Polytechnical University,

Xi'an 710072, China.

E-mail: mayue04@nwpu.edu.cn

1. Experimental Section

1.1. Materials preparation

1.1.1. Synthesis of AlO$_x$-MPE membrane

Firstly, we prepare the amorphous AlO$_x$ colloids by mixing the aluminum triacetate (0.2 M) solution with 5 wt % urea (CH$_4$N$_2$O, 97%) additive. Then, the aqueous solution was kept with the magnetic stirring at 90 °C for 2h. The coating slurry was prepared by mixing amorphous AlO$_x$ colloids and polyvinylidene fluoride (PVDF) surfactant (Chemwill Asia Co., Ltd) with a weight ratio AlO$_x$: PVDF=98:2. After that, the pristine polyethylene membrane (9 μm) was immersed in above AlO$_x$ colloids-PVDF suspension. The coated separators were dried at 60 ℃ for 2 h. The composited separators were thickened to 13 μm by repeated dip-coating and drying processes. The AlO$_x$-MPE separators were further vacuum-dried at 100 ℃ for 12 h prior to use.

1.1.2. Synthesis of N-doped Carbon foam

N-doped Carbon foam was prepared through a facile calcination process. Briefly, the commercial melamine foam (Sichuan SINOYQX Co., Ltd.) was tailored into small pieces and then were immersed in concentrated nitric acid for 12 hours. After this, they were washed by distilled water and ethanol and dried at 60 °C overnight. Then, these pieces were carbonized in tube furnace at 800 °C for 1 h with a heating rate of 4 °C min^{-1} in the flowing nitrogen atmosphere.[1] After cooling down, the product for N-doped carbon foam was obtained.

1.1.3. Synthesis of 1T-MoS$_2$/N-doped Carbon composites

The 1T-MoS$_2$/N-doped Carbon composite was synthesized through one-step hydrothermal process. Firstly, the precursor MoO$_x$ powder was prepared by the previous report.[2] Secondly,

0.40 g of MoO$_x$ powder and 0.30 g of thiourea were dissolved into 60 mL distilled water to form a homogeneous solution. After stirring for 6 h, the small pieces of carbon foam were soaked in the suspension and then hydrothermally treated at 200 °C for 48 h in the Teflon-lined stainless-steel autoclave. After that, the product was thoroughly washed with ethanol and water for three times, and dried in a vacuum oven for 12 hours. The final product was designated as 1T-MoS$_2$/NCF composite. For comparison purpose, the MoS$_2$ material without carbon foam was further synthesized through a one-step hydrothermal process mentioned above, while keeping other experimental details constant. In addition, other MoS$_2$/NCF composites were also prepared through the hydrothermal reaction at different temperature (160 °C, 180 °C and 220 °C), while keeping other experimental details constant. The as-obtained products were designated as MoS$_2$/NCF-160, MoS$_2$/NCF-180 and MoS$_2$/NCF-220, respectively. The preparation procedures of 2H-MoS$_2$/NCF were also elaborated. Briefly, the small pieces of carbon foam were soaked in the suspension and then hydrothermally treated at 220 °C for 48 h in the Teflon-lined stainless-steel autoclave. After washing with ethanol and water for three times and drying in a vacuum oven for 12 hours. the final product was designated as 2H-MoS$_2$/NCF composite.

1.1.4. Synthesis of NaVPO$_4$F (NVPF)

NVPF cathode materials were synthesized with a two-step solid-state method.[3-5] Firstly, V$_2$O$_5$, NH$_4$H$_2$PO$_4$, and C$_6$H$_{12}$O$_6$ with a molar ratio of 3:6:1 were employed to prepare VPO$_4$ intermediate precursor through a calcination process at 750 °C for 1 h in the flowing argon atmosphere. Secondly, the as-obtained VPO$_4$ precursor and NaF were mixed into a porcelain boat and then heat-treated at 750 °C for 4h in the argon atmosphere. Then the as-formed product

was designated as NVPF.

1.2. Materials characterization

The crystal structure and phase nature of 1T-MoS_2/NCF material were measured by X-ray diffraction (XRD, STOE) with CuKα radiation (λ= 1.5418 Å) ranging from 1° to 71° operating at the current of 40 mA and voltage of 40 KV. The morphology and microstructure of the products were studied by field-emission scanning electron microscopy (FE-SEM, FEI NovaSEM 450) with energy dispersive X-ray spectrometer (EDX) and transmission electron microscope (TEM, TF20, Joel2100F). The valence states and composition of as-prepared products were characterized by scanning X-ray photoelectron spectroscopy (XPS, Escalab 250XI, Thermo Fisher Scientific, UK) operated at 250 kV. Beyond that, the Raman spectrums were examined on a HORIBA Raman spectrometer (France) by using the 532-excitation beam/laser.

1.3. Characterization of AlO$_x$-MPE membrane

Na-ion transference number (t_{Na^+}) of the electrolyte-soaked AlO$_x$-MPE seoarator was evaluated by employing the steady-state current method.[6,7] On this basis, the coin cell was assembled by integrating two Na foils on both sides of AlO$_x$-MPE separator. This method contains the initial current (I_0), then applying a small voltage (DV, 10 mV) across the coin cell until a steady current (I_{ss}) is obtained. Additionally, the Na-ion transference number is approximately calculated by using the equation:

$$t_{Na^+} = \frac{I_{ss}}{I_0}$$

(1)

The ionic conductivity (δ) of the AlO$_x$-MPE separator was characterized by using

electrochemical impedance spectroscopy (EIS), where the coin cell (stainless steel/AlO$_x$-MPE separator/stainless steel) was assembled by integrating the liquid electrolyte-soaked AlO$_x$-MPE separator between two stainless-steel spacers. Furthermore, the ionic conductivity of the separator is obtained by using the equation:

$$\delta = \frac{d}{R_b S}$$

(2)

Where d is the thickness of the separator, R$_b$ is the bulk resistance of the separator and S is the area of the separators. Besides, the tensile strength was conducted by a tensile tester (Instron 5942). For the wettability measurements to the AlO$_x$-MPE membrane, the contact angles were measured using a drop shape analyzer (DSA-100, KRUSS, Germany).

1.4. Electrochemical Measurements

The working electrodes were prepared by using spin-coating method. Firstly, after grinded with mortar, the active material, super P and carboxymethylcellulose (CMC) were mixed with the weight ratio controlled as 70:20:10, which were then suspended in deionized (DI) water to make a slurry and cast uniformly on a copper foil. After that, the coated copper foil was dried at 60 °C overnight and then cut into circular pieces with a diameter of 12 mm. For the CR2032 coin-type cells, the dried electrode was employed as the working electrode, sodium metal foil as the counter electrode separated by the AlO$_x$-MPE separator and the NaClO$_4$ solution (1 M) in ethylene carbonate and dimethyl carbonate (1:1 by volume) with 5 vol% additive fluoroethylene carbonate as the electrolyte. All the fabrication process was assembled in a glove box with filled argon atmosphere (Universal, Mikrouna, Germany).

The commercial PE membrane (9 μm) was modified by AlO$_x$ layer. The nano AlO$_x$ layers with a thickness of 2 μm were coated on both sides of PE membarne by micro-curve coating in

the present of binder.[8] Besides, this modified separator was used as the structural support and separator. The anode slurry was coated onto a AlO_x-MPE separator with the pre-designed loading mass as an electrode (namely 1T-MoS_2/NCF-S) through spin-coating process. And the cathode slurry was also cast on the AlO_x-MPE separator as an electrode (namely NVPF-S) for half-cell. Similarly, the integrated NVPF (cathode)-AlO_x-MPE-1T-MoS_2/NCF (anode) film could also be integrated via spin-coating method.

During the galvanostatic charge/discharge test, the cells for anode were conducted with a voltage window of 0.001 ~ 2.6 V on a Neware electrochemical station. Furthermore, the various current rates were applied to measuring the rate capacity in the voltage window from 0.001 to 2.6 V. And the cells for cathode were discharged/charged in the voltage window between 2.8 and 4.2 V at a current rate of 0.15 C.

The full cells were fabricated by integrating the anode and NVPF cathode electrode with aluminum plastic film. The galvanostatic charge/discharge tests were operated from open circuit voltage (OCV) to 4 V, while the following cycles was between 4 V and 1 V.
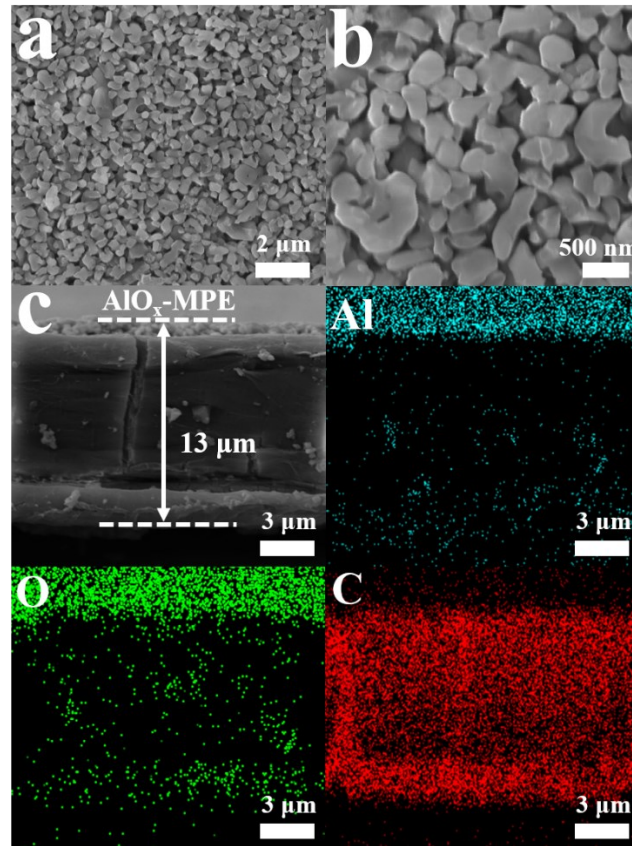
Fig. S1 (a), (b) The top-view FESEM images of AlO$_x$-MPE separator. (c) Cross-sectional SEM images and EDX-mapping of Al, O and C elements of AlO$_x$-MPE Separator.
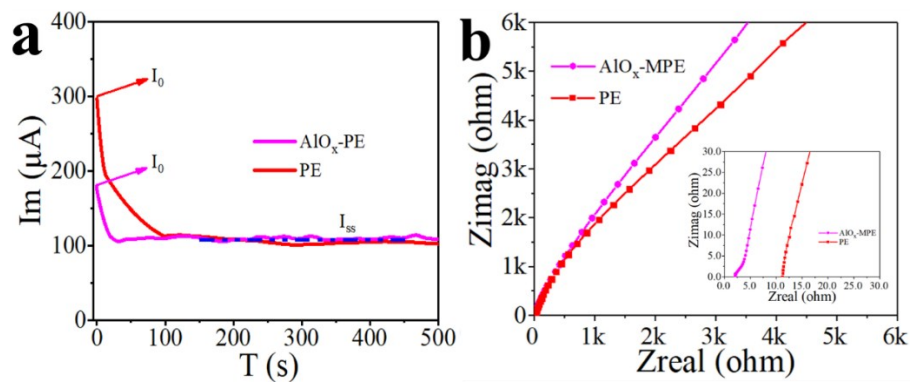

Fig. S2 (a) Na-ion transference number Measurement of the Na/AlO$_x$-MPE separator/Na and Na/PE separator/Na coin cell by Chronoamperometry at a potential step of 10 mV. (b) Nyquist plots of the coin cells (stainless steel/separator/stainless steel) for the liquid electrolyte-soaked AlO$_x$-MPE separator and PE separator.
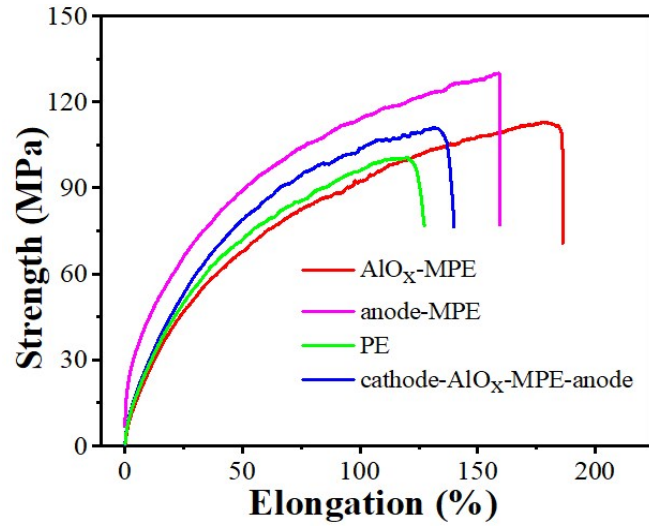
Fig. S3 The tensile properties of PE separator, the AlO_x-MPE separator, anode-MPE film and

cathode-AlO_x-MPE-anode film.
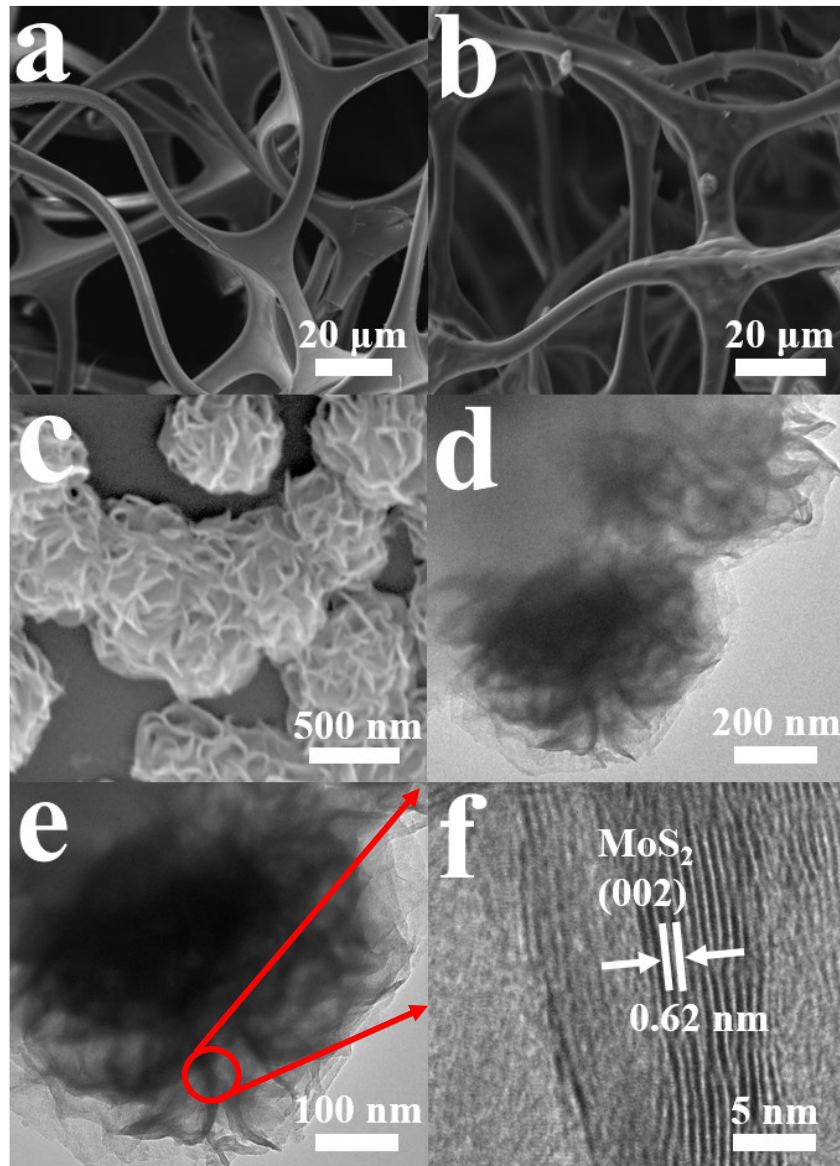
Fig. S4 Top-view SEM images of (a) MF, (b) NCF, (c) as-formed pure MoS_2 nanosheets. (d), (e) TEM image of pure MoS_2 nanosheets. (f) HRTEM image of pure MoS_2 nanosheets.
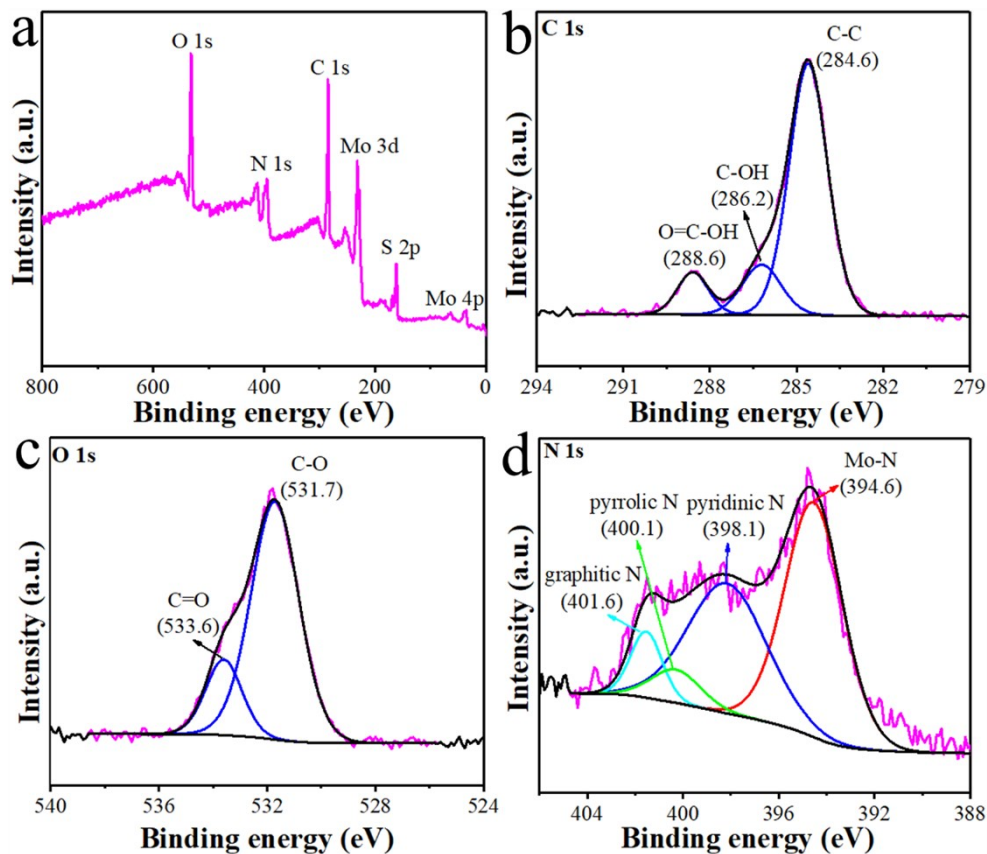
Fig. S5 High resolution X-ray photoelectron (a) Survey, (b) C 1s, (c) O 1s, (d) N 1s spectrum

of 1T-MoS$_2$/NCF composite.

The Survey XPS spectra of 1T-MoS$_2$/NCF shown in Fig. S5a, verifies that the co-presence

of Mo, S, C, N and O elements in the composite. Fig. S5b demonstrates that the C 1s peak

positioned at 284.8 eV, 286.2 and 288.6 eV for C-C bonding, C−OH and O=C-OH groups,

respectively.[9,10] The O 1s core-level spectrum exhibits the two dominant peaks at 531.7 and

533.6 eV, which are the characteristics for C-O bonding and C=O bonding, respectively (Fig.

S5c).[11] The N1s core-level spectrum is deconvoluted into four different peaks: 394.6 ev for Mo-

N, 398.1 ev for pyridinic nitrogen, 400.1 eV pyrrolic nitrogen and 401.6 eV for graphitic

nitrogen, respectively, demonstrating the successful nitrogen doping in NCF upon the pyrolysis

(Fig. S5d).[12,13]
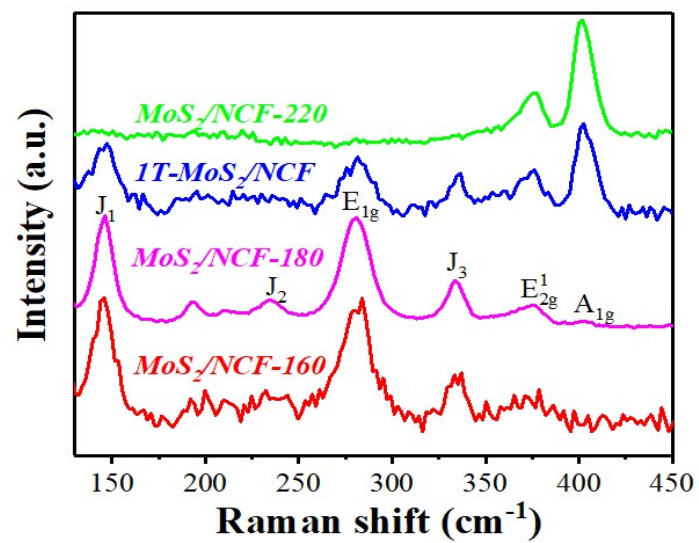
Fig. S6 Raman spectra of various MoS$_2$/NCF composites synthesized at different hydrothermal temperature.
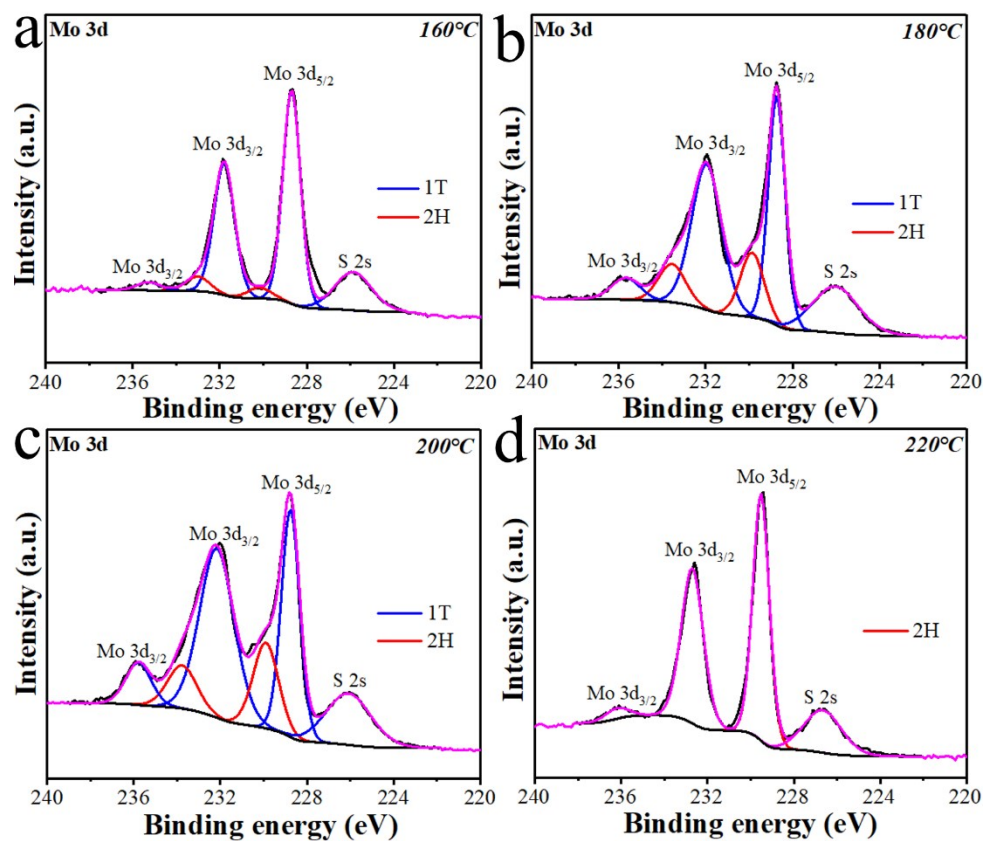
Fig. S7 The XPS spectrums of the various MoS$_2$/NCF composites synthesized at different hydrothermal temperature, (a) 160℃, (b) 180℃, (c)200℃, (d)220℃.
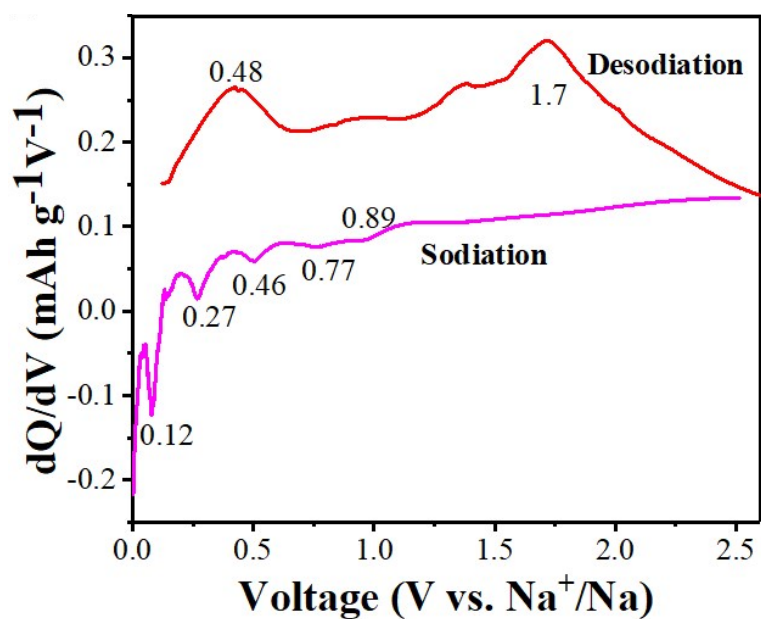
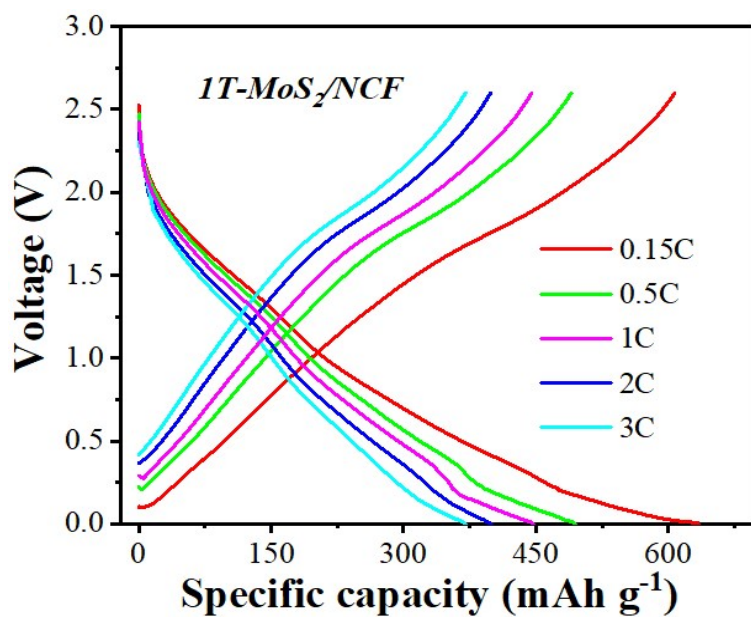Fig. S8 The dQ/dV curve of the 1T-MoS$_2$/NCF electrode at the first cycle.

Fig. S9 The discharge-charge profiles of the 1T-MoS$_2$/NCF electrode at the different rates.
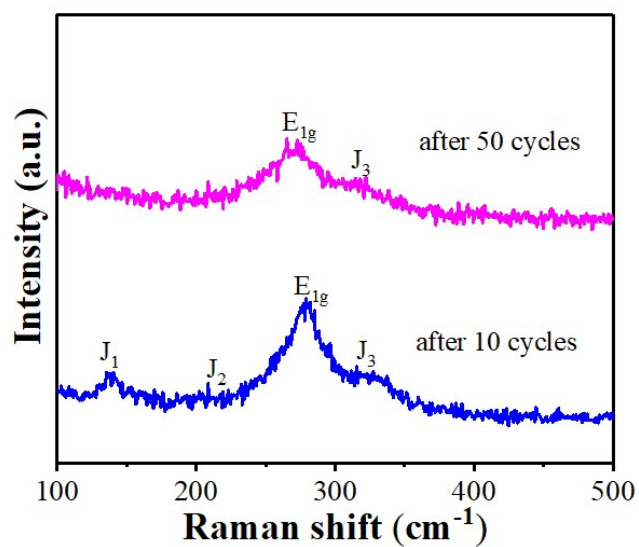
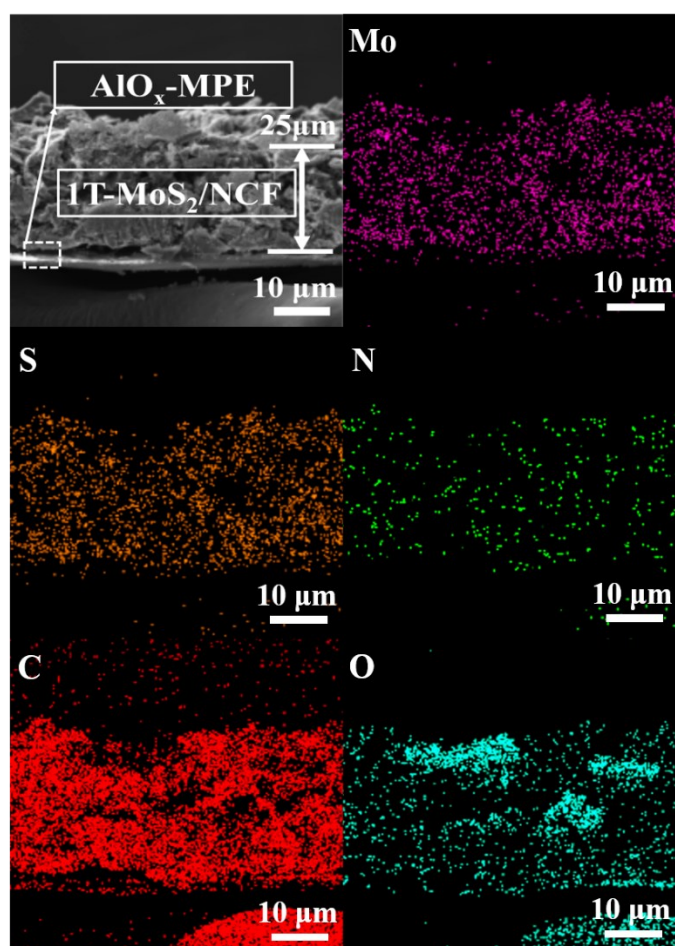Fig.S10 Raman spectra of 1T-MoS$_2$/NCF electrode at different cycles.

Fig. S11 The cross-section SEM image and corresponding EDX-mapping of Mo, S, P, N, C, and O elements of anode-AlO$_x$-MPE (1T-MoS$_2$/NCF-S) film.
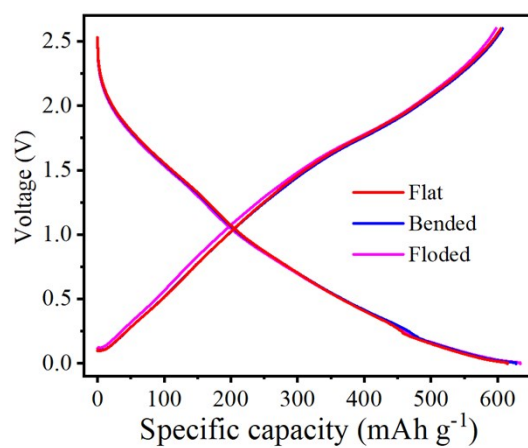
Fig. S12 Charge-discharge profiles of the 1T-MoS$_2$/NCF-S film under different flexing states.
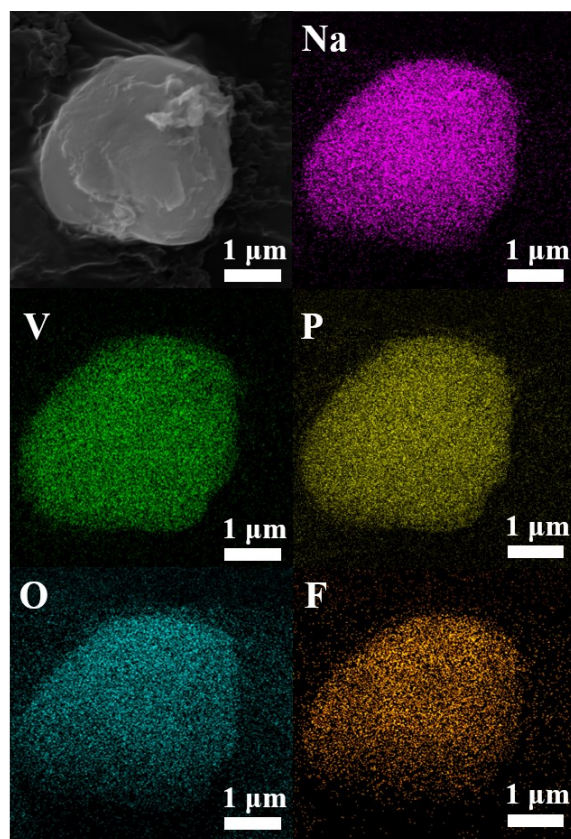
Fig. S13 Top-view SEM image and EDX-mapping of Na, V, P, O, F elements of as-prepared NVPF particle.

The morphology characterization of cathode materials is exhibited in Fig. S13. Fig. S13 shows the SEM image of NVPF cathode, demonstrating that the small particle is ellipsoidal with a size of approximately 2 μm. Meanwhile, the EDX mapping reveals the uniform distribution of Na, V, P, O, F elements, validating the ellipsoidal shape of as-prepared NVPF particle (Fig. S13).
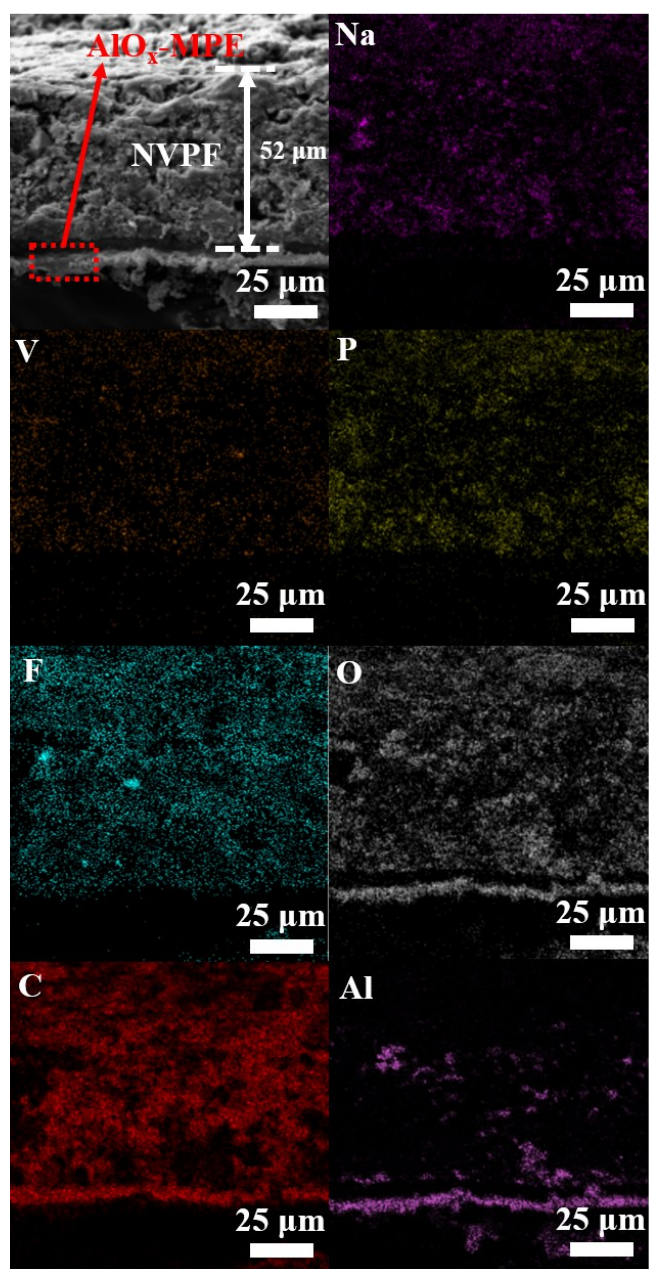
Fig. S14 Cross-sectional SEM image and EDX-mapping of Na, V, P, F, O, C, and Al elements of cathode-AlO$_x$-MPE (NVPF-S) film.

The cathode slurry was cast on the AlO$_x$-MPE separator as an electrode through spin-coating process (namely NVPF-S). As shown in Fig. S14, the cross-sectional SEM image of NVPF-S electrode exhibits the controlled thickness of cathode slurry layer as 52 μm. Besides,

the EDX-mapping verifies the uniform distribution of Na, V, P, F, C, O, and Al elements on the integrated NVPF-S electrode.
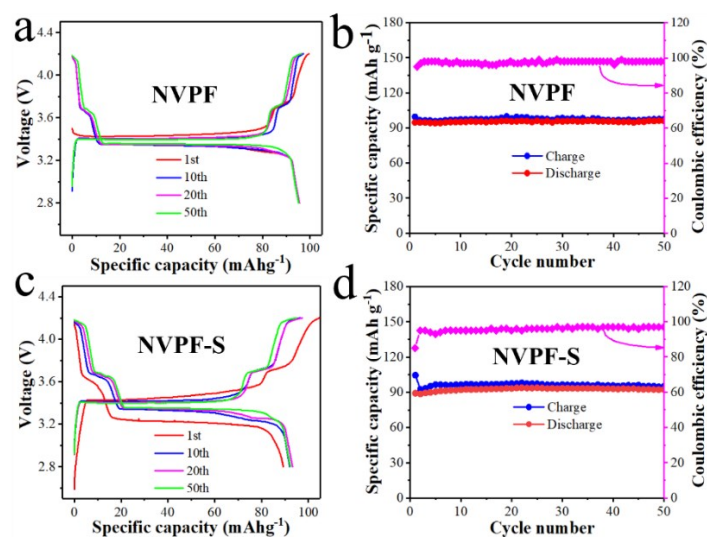

Fig. S15 The electrochemical characterization of the NVPF cathode. (a) The charge/discharge curves of NVPF electrode. (b) Cycling behavior of NVPF electrode. (c) The charge/discharge curves of NVPF-S electrode. (d) The cycling behavior of NVPF-S electrode

The electrochemical characterization of cathode materials are displayed in Fig. S15. Fig. S15a exhibits the overlapped charge/discharge profiles of NVPF cathode during the 1st, 10th, 20th, 50th at 0.15 C (1 C = 0.14 A g^{-1}) with a voltage window of 2.8~4.2 V. All the charge/discharge profiles have flat plateaus approximately at 3.4 V, corresponding to the reversible Na ions insertion/extraction into NVPF cathode.[14] However, NVPF also exhibits a small plateau at 3.7 V due to its impurity. When galvanostatically charged and discharged at 0.15 C (Fig. S15b), NVPF electrode displays a reversible specific capacity of 97.5 mAh g^{-1} with a high CE (>98%) over 50 cycles, demonstrating its excellent cycling stability. The superimposable charge/discharge curves show the typical sodiation/desodiation characters of NVPF-S electrode, and thus verify the structural stability of NVPF-S electrode. (Fig. S15c).

The cycling performance of integrated NVPF-S electrode is tested at 0.15 C (Fig. S15d): NVPF-S electrode displays a reversible specific capacity of 95 mAh g^{-1} with a high CE (>97%) over 50 cycles.
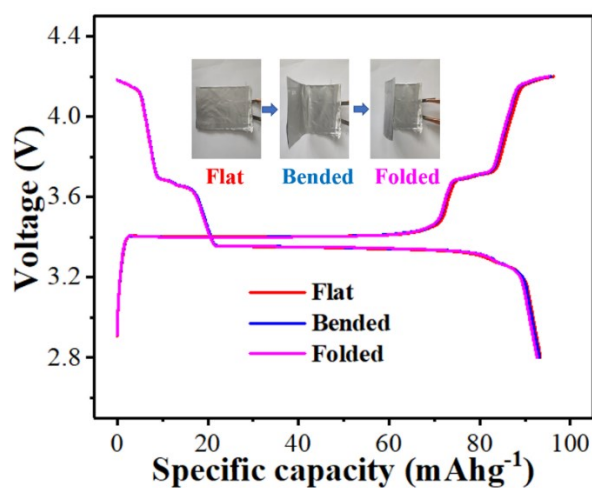

Fig. S16 Charge-discharge profiles of the NVPF-S film under different flexing states.

Fig. S16 exhibits the overlapped charge–discharge curves for NVPF-S electrode at the flat, bended, and folded states, testifying its superior structural robustness and mechanical flexibility.
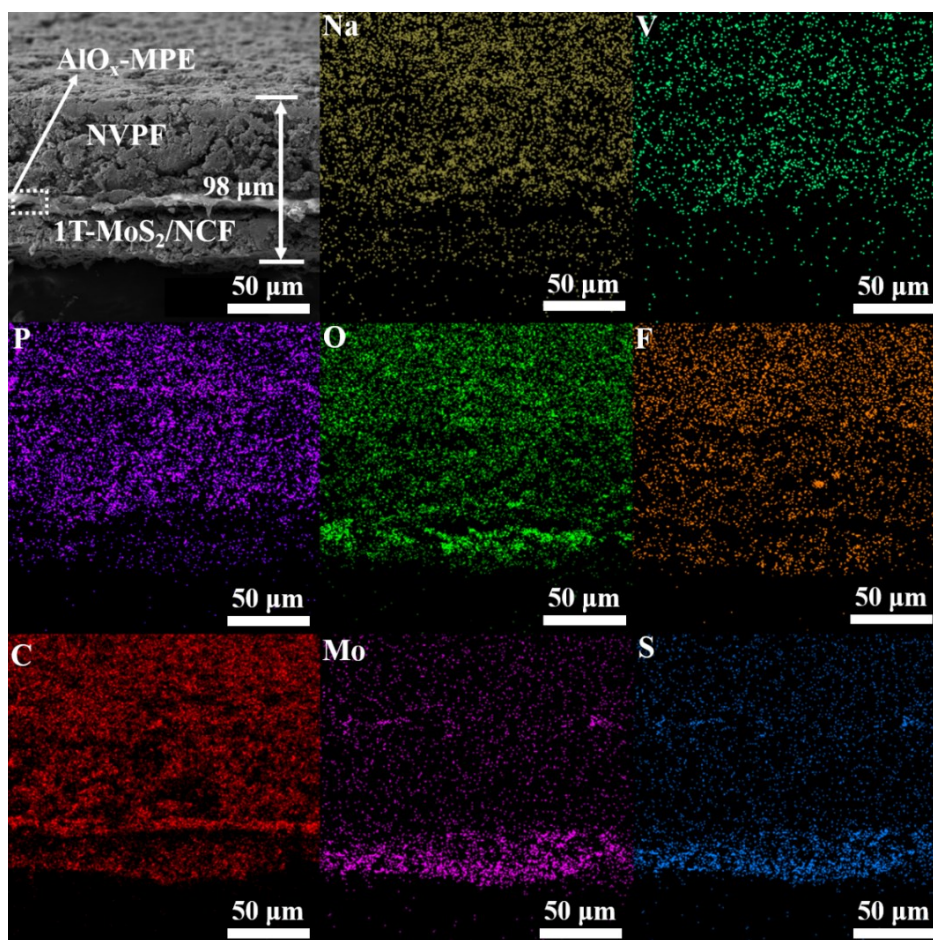
Fig. S17 Cross-sectional SEM image and EDX-mapping of Na, V, P, O, F, C, Mo, and S elements of the integrated, sandwich-like cathode-AlO$_x$-MPE-anode film.
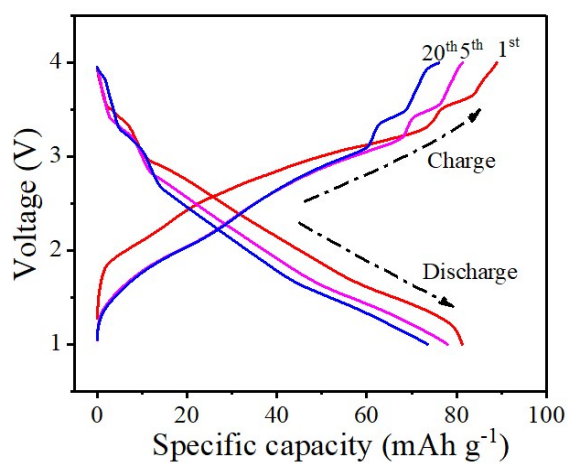

Fig. S18 The 1st, 5th, 20th charge-discharge profiles of the full cell at 0.5 C.
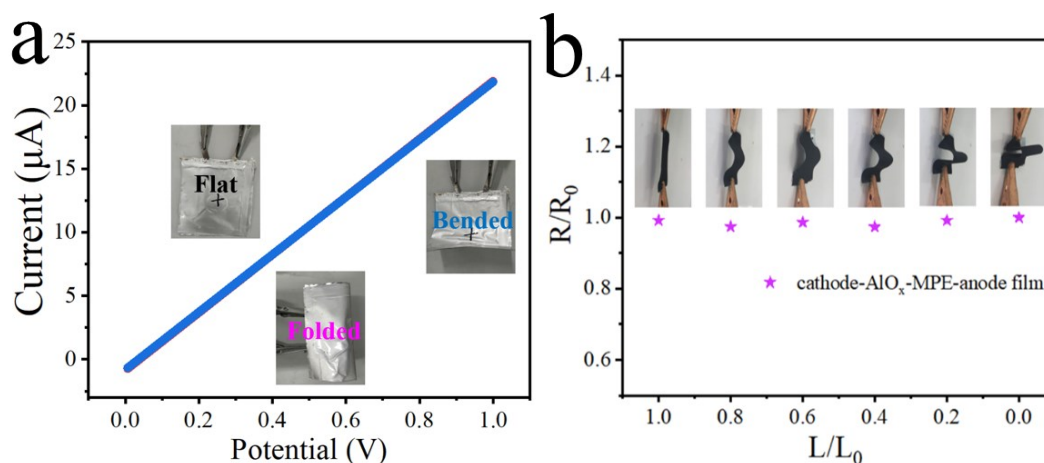
Fig. S19 (a) The electrical conductivity of the integrated film under different bending states.

(b) The R/R_0 values of the integrated cathode-AlO_x-MPE-anode film at different bending states.

Table S1 Comparison of energy/power densities of different sodium ion full cells.

Full cell Cathode‖Anode	Rate (C)	Energy density (Wh kg^{-1})	Power density (W kg^{-1})	Ref.
$Na_3Ni_2SbO_6$‖Sb-C	0.1	210	21	[72]
$NaCrO_2$‖Sb-C	0.1	180	18	[73]
$[NaCu_{1/9} Ni_{2/9} Fe_{1/3} Mn_{1/3}]O_2$‖hard carbon	0.1	215	21.5	[74]
	0.5	197	98.5	
	1	186	186	
$Na_3V_2(PO_4)_2F_3$‖hard carbon	0.2	290	58	[75]
$Na_3V_2(PO_4)_3$‖3D graphene	0.1	171.2	17.12	[76]
NaFePO$_4$@C nanofibers‖carbon	0.5	168.1	84.05	[77]
$NaVPO_4F$‖1T-MoS$_2$/NCF	0.5	196.79	98.396	This work
	1	161.60	161.60	
	2	146.68	293.35	
	4	127.56	510.23	
	10	93.27	932.66	
	20	52.45	1048.91	

Reference

1 R. Tjandra, W. W. Liu, L. Lim, A. P. Yu, *Carbon*, 2018, **129**, 152-158.

2 L. C. Yang, S. N. Wang, J. J. Mao, J. W. Deng, Q. S. Gao, Y. Tang, O. G. Schmidt, *Adv. Mater.*, 2013, **25**, 1180-1184.

3 Y. Lu, S. Zhang, Y. Li, L. G. Xue, G. J. Xu, X. W. Zhang, *J. Power Sources* **2014**, *247*, 770-777.

4 M. Law, P. Balaya, *Energy Storage Mater.*, 2018, **10**, 102-113.

5 B. Cheng, S. J. Zhang, F. X. Zou, L. L. Luo, Y. X. Chen, S. J. Chen, H. T. Zhuo, X. R. Zeng, *J. Alloys Compd.*, 2019, **811**, 151828.

6 Z. Q. Jin, K. Xie, X. B. Hong, Z. Q. Hu, X. Liu, *J. Power Sources*, 2012, **218**, 163-167.

7 J. Choi, G. Cheruvally, D. Kim, J. Ahn, K. Kim, H. Ahn, *J. Power Sources*, 2008, **183**, 441-445.

8 R. J. Pan, Z. H. Wang, R. Sun, J. Lindh, K. Edström, M. Strømme, L. Nyholm, *J. Materiomics*, 2019, **5**, 204.

9 P. Burg, P. Fydrych, D. Cagniant, G. Nanse, J. Bimer, A. Jankowska, *Carbon*, 2002, **40**, 1521-1531.

10 F. Zhang, T. F. Zhang, X. Yang, L. Zhang, K. Leng, Y. Huang, Y. S. Chen, *Energy Environ. Sci.*, 2013, **6**, 1623-1632.

11 L. Wang, Y. Y. Fu, Y. Q. Fu, Y. F. Li, R. H. Zhou, S. H. Chen, Y. H. Song, *J. Alloys Compd.*, 2017, **724**, 1117-1123.

12 J. Y. C. Qiu, Z. X. Yang, Q. Li, Y. Li, X. Wu, C. Y. Qi, Q. D. Qiao, *J. Mater. Chem. A*, 2016, **4**, 13296-13306.

13 Z. H. Wang, Q. Long, L. X. Yuan, W. X. Zhang, X. L. hu, *Carbon*, 2013, **55**, 328-334.

14 X. C. Ge, X. H. Li, Z. X. Wang, H. J. Guo, G. C. Yan, X. W. Wu, J. X. Wang, *Chem. Eng. J.*, 2019**, 357***, 458-462.